GEOPHYSICAL RESEARCH LETTERS, VOL. 23, NO. 7, PAGES 705-708, APRIL 1, 1996

Transport in sandstone: A study based on three dimensional microtomography

F. M. Auzerais[1], J. Dunsmuir[2], B. B. Ferréol[3], N. Martys[4], J. Olson[3], T. S. Ramakrishnan[1], D. H. Rothman[3], and L. M. Schwartz[1]

Abstract. High resolution imaging of the microstructure of Fontainebleau sandstone allows a direct comparison between theoretical calculations and laboratory measurements. While porosity, pore-volume-to-surface ratio, permeability, and end point relative permeability are well predicted by our calculations, we find that electrical resistivity and wetting phase residual saturation are both overestimated.

Introduction

Transport in porous media is of importance in biology, chemical engineering, earth and environmental sciences, materials science, and physics [*Adler,* 1992; *Cushman,* 1990]. Because real porous media are usually highly disordered, most recent work on transport theory has been based on synthetic model systems, such as random sphere packs [*Adler,* 1992; *Schwartz et al.,* 1993]. Although instructive, such studies are not easily applied to the understanding of real materials. High resolution synchrotron microtomography [*Flannery et al.,* 1987; *Kinney et al.,* 1993; *Schwartz et al.,* 1994; *Spanne et al.,* 1994 *Coles et al.,* 1995] however, may be used to map the pore space of a real material. Here we study the geometrical and transport properties of three-dimensional tomographic reconstructions of several samples of Fontainebleau sandstone. We compare numerical calculations to laboratory measurements made on samples approximately an order of magnitude larger in linear dimension. We obtain a heirarchy of results, presented in Table 1. Geometrical properties are accurately estimated by our calculations, as is the permeability to single-phase flow. The computed electrical conductivity, on the other hand, underestimates the experimental results. Studies of immiscible displacement by a non-wetting fluid give mixed results. While our endpoint relative permeability calculation is in good agreement with the measured data, the corresponding saturation is less satisfactory.

[1]Schlumberger-Doll Research, Ridgefield, CT.
[2]Exxon Research and Engineering Company, Annandale, NJ.
[3]Department of Earth, Atmospheric and Planetary Sciences, Massachusetts Institute of Technology, Cambridge, MA.
[4]National Institute of Standards and Technology, Building Materials Division, Gaithersburg, MD.

Paper number 96GL00776
0094-8534/96/96GL-00776$03.00

Methodology

Laboratory Measurements: A cylindrical core, approximately 20 mm diameter and 37.5 mm long, was vacuum dried at 80 °C and the porosity, ϕ, was measured by He intrusion and buoyancy techniques and found to be 0.152 ± 0.002. Magnetic resonance measurements [*Hurlimann et al.,* 1994] of the pore volume to surface area ratio, V_p/S, gave $V_p/S = 9.6$ μm. Permeability to dry nitrogen was found to be 1.116 μm^2. The sample was then equilibrated with aqueous solutions of five different salinities and the electrical resistivity was measured with a four-terminal impedance meter. The effective electrical conductivity, σ_{eff}, of the sample was found to be linearly related to the solution conductivity and the formation factor, $F = \sigma_{fl}/\sigma_{eff}$, where σ_{fl} was the conductivity of the pore fluid, was calculated to be 25.6 ± 0.2. *Liquid permeabilities* of 1.059 μm^2 and 1.073 μm^2 were obtained for two different solutions of resistivities 1 Ωm and 0.26 Ωm, respectively. Lastly, the core was injected with oil to the point of residual water saturation S_{rw}. (S_{rw} is the fraction of the pore space occupied by water when water can no longer be expelled from the core.) We then measured [*Ramakrishnan and Cappiello,* 1991] the *relative* permeability k^0_{ro}, the ratio of the permeability to oil of this mostly oil filled sample to the single phase permeability, and found $k^0_{ro} = 0.92$. The measured value of S_{rw} was 0.03.

X-ray Microtomography: Two cylindrical plugs 3.5 mm in diameter were cut adjacent to the sample used for laboratory measurements. Our imaging technique is based on second generation protocols that employ *parallel* data acquisition based on two dimensional detectors [*Flannery et al.,* 1987; *Kinney et al.,* 1993]. The principal advantage of this technique is that it yields symmetric data sets in which each of the three directions is treated on an equal footing. By contrast, other studies of this kind [*Spanne et al.,* 1994; *Coles et al.,* 1995] have been based on first generation techniques in which three dimensional data is collected by the successive imaging of two dimensional planes. From the first plug we extracted a data cube of attenuation coefficients of size 224×288^2 (Sample 1) with a voxel edge of 7.5 μm and from the second plug we worked with two contiguous samples (Samples 2 & 3) of size 235×288^2. The left-hand panel of Figure 1 shows a gray-scale image of the attenuation coefficients, α, in a 2D slice of size 288^2. To separate the void space from

Table 1. Measured and calculated values of porosity ϕ, pore-volume-to-surface ratio V_p/S (in μm), formation factor F, permeability k (in $(\mu m)^2$), endpoint relative permeability k^0_{ro}, and residual saturation S_{rw}. In the first column the numbers in parenthesis denote the sample on which the calculations were based; in the permeability column, FD and LB denote values computed by finite-difference and lattice-Boltzmann methods, respectively. The endpoint relative permeabilities were computed from both nonwetting invasion (Type I) and constant saturation (Type II) simulations.

	ϕ (%)	$\frac{V_p}{S}$	F	k	k^0_{ro}	S_{rw}
Exp	15.2	9.6	25.6	1.1	0.92	0.03
Cal (1)	16.8	10.4	36.0	1.0 (FD)	0.84 (I)	0.53
				1.2 (LB)	0.90 (II)	
Cal (2)	15.0	8.9	28.6	1.3 (FD)	—	—
Cal (3)	14.6	8.7	32.7	1.0 (FD)	—	—

the rock matrix, a threshold, α_c, could be specified by simply requiring that α_c produce the measured porosity [*Spanne et al.*, 1994]. However, the quality of the present images is such that we can predict (i.e. calculate) α_c using a least squares estimate that preserves the mean attenuation coefficient of (i) the entire image and (ii) the pore and grain sub-populations [*Magid, et al.*, 1990]. The method was applied to all three samples to yield a mean value of 0.154, in excellent agreement with the porosity measured on the larger core. The right-hand panel of Figure 1 shows the left-hand panel after the computed threshold was applied to create a binary image. An image of a small part of the 3D pore space is shown in Figure 2. We also computed the pore volume to surface area ratio, V_p/S, by counting pore sites and voxel surfaces that separate pore from solid sites, and obtained results within 10% of experimental measurements. This agreement is gratifying because the resolution of the magnetic resonance measurements is 5 μm, essentially the same as our microtomography.

Theoretical Calculations: To calculate electrical conductivity we employ random walk techniques to simulate diffusion in the 3D pore space [*Schwartz et al.*, 1993]. The random walk step length, ϵ, was one third of the voxel edge and our results did not change significantly with a further reduction of ϵ. Our calculations on all three samples consistently overestimated F by 20–50%.

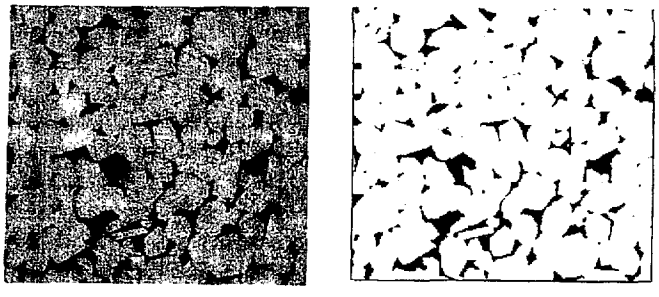

Figure 1. Left hand panel shows a gray-scale image obtained by X-ray microtomography with a voxel edge length of 7.5 μm. The corresponding binary representation of this image is shown in the right hand panel.

Figure 2. The pore space within a 64^3 sub-volume of Sample 1.

Permeability to fluid flow in a given direction is defined by Darcy's law [*Adler*, 1992]

$$Q = -\frac{k}{\eta}\left(\frac{\Delta P}{L} - \rho g\right) \quad , \tag{1}$$

where ΔP is an applied pressure difference across a porous sample of length L, ρg is a body force (e.g., gravity) per unit volume, Q is the macroscopic volumetric flux of fluid per unit area, η is the fluid's viscosity, and k is the permeability, which has the dimensions of area. To calculate k from first principles, we solved the Stokes equations, which describe creeping fluid flow, by two different methods, a classical finite difference technique [*Schwartz et al.*, 1993] and a "lattice-Boltzmann" method [*Benzi et al.*, 1992]. The former is a direct numerical integration of the partial differential equations whereas the latter solves a discretized Boltzmann equation that is equivalent, macroscopically, to solving the Stokes equations. Both methods determined permeabilities that were in the range 1.0–1.3 μm^2, in good agreement with measurements.

Interestingly, the size of our tomographic samples, about seven grains on a side, is close to the minimum size required to estimate the permeability with acceptable accuracy. To show this, we compare in Figure 3 the computed porosity and permeability in 64 distinct subcubes of size 56^3, 8 distinct subcubes of size 112^3, and larger subcubes of size greater than or equal to 224^3. The porosity varies over approximately a factor of four for the smallest samples, over about 10% for the intermediate samples, and insignificantly for the largest samples. Thus the intermediate size seems acceptable for estimates of porosity. The permeability fluctuations, on the other hand, range over nearly *three* orders of magnitude for the smallest samples, by a fac-

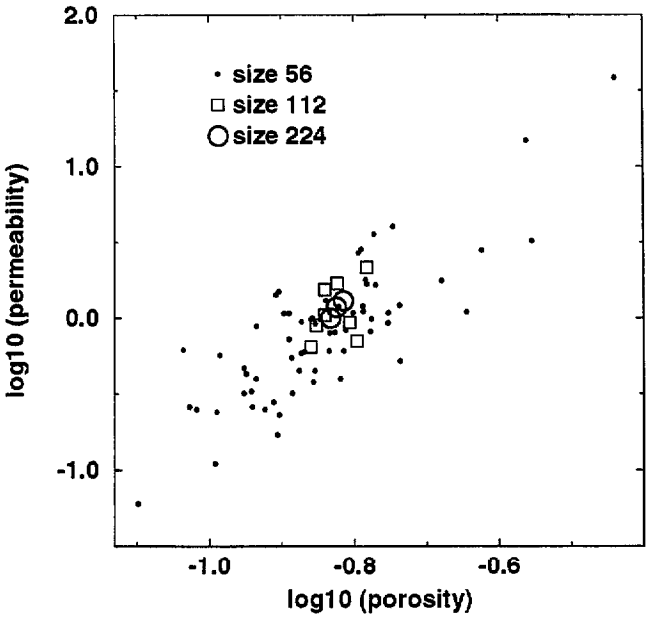

Figure 3. Calculated permeabilities are shown for sub-volumes of Sample 1 (using a lattice-Boltzmann method) of three different sizes [*Ferréol and Rothman,* 1995] in addition to calculated permeabilities for samples 2 and 3 (using a finite-difference method).

tor of two for intermediate samples, and by about 30% for the largest samples. The scatter in the smaller samples is also roughly consistent with the results reported by Spanne et al. [*Spanne et al.,* 1994]. (Their study was limited to 5 distinct samples whose size ranged from 44^3 to 84^3 with a resolution of 10 μm rather than 7.5 μm.)

Relative permeability, on the other hand, may exhibit much stronger size dependencies. To investigate this point, we performed two simulations based on a 3D *immiscible lattice-gas* model [*Olson and Rothman,* 1995], an extension of earlier 2D models. In our two-fluid model, one fluid perfectly wets the solid boundaries and the viscosities and densities in each fluid are equal. To save computation time, simulations were performed only on a subset of size 104^3 of Sample 1; a mirror reflection of the medium was applied in the flow direction to create periodic boundaries and a computational domain of size $104^2 \times 208$. The first simulation (Type I) imitated the immiscible displacement experiment: nonwetting fluid was injected into one face of the sample, which was initially filled with wetting fluid. The simulation is illustrated in Figure 4. To make the flow periodic while always injecting nonwetting fluid, any wetting fluid that left the outlet was reinjected as nonwetting fluid at the inlet. The flow rate of the nonwetting fluid was calculated by averaging its velocity over the entire sample when the wetting fluid could no longer be evacuated; k_{ro}^0 was then computed from the two-phase generalization of Eq. (1) [*Adler,* 1992]. Our result, $k_{ro}^0 = 0.84$, is in reasonable accord with measurements, but the calculated residual (wetting phase) saturation, $S_{rw} = 0.53$, is not. The second simulation (Type II) followed previous studies of artificial media in which the pore space is initially filled with a homogeneous mixture of wetting and nonwetting fluid of specified relative saturations [*Gunstensen and Rothman,* 1993]. The mixture is then forced through the rock with fully periodic boundary conditions in the flow direction. Only the nonwetting fluid is forced, and the two fluids undergo phase separation as they flow. The flow rate of the nonwetting fluid is then computed in the steady state. When the saturation is specified to be the measured residual saturation $S_{rw} = 0.03$, we find $k_{ro}^0 = 0.90 \pm 0.02$, in good accord with measurements.

Discussion

Our calculations give excellent approximations for the geometrical parameters ϕ and V_p/S, the permeability k,

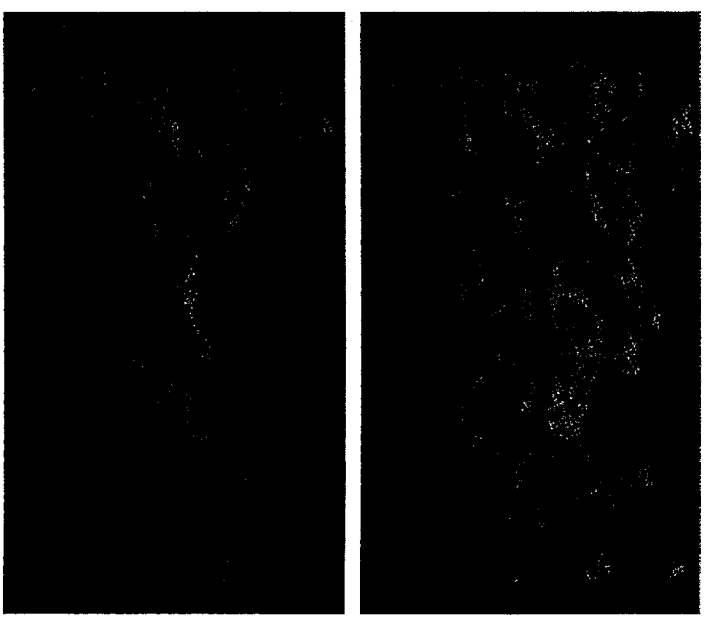

Figure 4. Simulation of invasion of nonwetting fluid into Sample 1, which was initially filled with wetting fluid. The invading fluid enters the sample at the top; the sample is viewed from above and to the left. The background is black, the solid porous matrix is transparent and colorless, the wetting fluid is transparent and blue, and the nonwetting fluid is opaque and red. Thus black also indicates that the solid matrix is contiguous in the line of sight. The left-hand panel shows the breakthrough configuration and the right-hand panel shows the configuration of the nonwetting fluid near steady state. Because the sample is jacketed by solid walls, which are themselves covered by a thin layer of wetting fluid, the left and right edges of the image (which correspond to only a small fraction of the total volume) are dominated by blue wetting fluid.

and the endpoint relative permeability k_{ro}^0. The calculations of electrical resistivity and residual saturation are less successful. A likely explanation for our underestimate of the effective conductivity is that, in addition to the current carried in the main large channels through the pore space, a significant part of the current is being carried in parallel channels that are smaller than the 7.5 μm resolution of the present images. The contribution of these smaller channels to current flow depends on their connectivity being properly described in the image, rather than just their contribution to the net porosity or total surface area [*Schwartz*, 1993]. Fluid flow, on the other hand, is a considerably less "democratic" transport process, and is controlled by the largest connected channels. In this connection, we note that the calculated values of F reported by Spanne *et al.* also tend to overestimate the experimental results. However, because those calculations were based on much smaller samples, it was not clear whether the problem was associated with finite size effects or image resolution.

The limiting factor in our relative permeability calculations appears to be a combination of the small sample size and the poor spatial resolution of the simulation. The latter problem manifests itself as a wetting layer that is too thick (i.e., about one lattice unit) relative to the radius of a typical pore or throat. Specifically, because 54% of the void sites in Sample 1 are adjacent to solid sites, our residual saturation of 53% could be consistent with drainage of nearly all wetting fluid except that adjacent to pore walls, and is therefore not necessarily inconsistent with the experimental value of 3%. This conclusion is supported by the observation that our theoretical estimate of the end-point relative permeability is good, since sites adjacent to walls contribute only marginally to the bulk flow. Evidence for the first problem—finite-size effects—is seen in Figure 4; when breakthrough of the nonwetting fluid occurs, one flow path strongly dominates the flow. It is clear from the dominance of this single flow path at breakthrough that the results cannot be easily scaled upwards. We emphasize that neither of these problems represent intrinsic limitations of either the tomographic reconstruction or our theoretical methods.

In conclusion, we note that the pursuit of issues such as the scale dependence and influence of heterogeneities on transport is one of the most promising future applications of studies such as ours. Indeed, this approach may be the most effective way to determine the physical mechanisms responsible for anomalous scaling of transport properties in sedimentary rocks [*Adler*, 1992; *Cushman*, 1990].

Acknowledgments. LMS acknowledges the support of NIST and Lawrence Livermore National Laboratory. Work at MIT was supported in part by NSF Grant 9218819-EAR, the sponsors of the MIT Porous Flow Project, Elf Aquitaine, and the the Petroleum Research Fund, administered by the ACS. The authors also acknowledge the Advanced Computing Laboratory of Los Alamos National Laboratory.

References

Adler, P., *Porous Media: Geometry and Transports*, Butterworth/Heinemann, 1992.

Benzi, R., Succi, S., and Vergassola, M., The lattice boltzman equation: theory and applications, Phys. Rep. *222*, 145-197, 1992.

Coles, M. E., Hazlett, R. D., Muegge, E. L., Furr, M. J., and Spanne, SPE 30542, Characterization of Reservoir core using computed microtomography, Presented at the Annual Technical Conference and Exhibition of the Society of Petroleum Engineers, October 22-25, 1995, Dallas, TX.

Cushman, J. H. (Editor) Dynamics of Fluids in Hierarchical Porous Media, Acdemic Press, San Diego, 1990.

Ferréol, B. and Rothman, D. H., Lattice-Boltzman simulations of flow through Fountainebleau sandstone, Transport in Porous Media, 1995 (in press).

Flannery, B. P., Deckman, H. W., Roberge, W. G., and D'Amico, K. L., Three-dimensional X-ray microtomography, Science *237*, 1439-1444, 1987.

Gunstensen, A. K. and Rothman, D. H., Lattice-Boltzman studies of two phase flow through porous media, J. Geophys. Res. *98*, 6431-6441 1993.

Hurlimann, M. D., Helmer, K. G., Latour, L. L., and Sotak, C. H., Restricted diffusion in sedimentary rocks: Determination of surface-area-tovolume ratio and surface relaxivity, J. Magnetic Resonance, A *111*, 169-178, (1994).

Kinney, J. H., Breunig, T. M., Starr, T. L., Haupt, D., Nichols, M. C., Stock, S. R., Butts, M. D., and Saroyan, R. A., X-ray tomographic study of chemical vapor infiltration processing of ceramic composites, Science *260*, 789-792, 1993.

Magid, A., Rotman, S. R., and Weiss, A. M. IEEE Trans. Systems, Man, and Cybernetics, *20* 1238-1239 (1989).

Olson, J., and Rothman, D. H., A three dimensional lattice-gas: application to sheared phase separation, J. Stat. Phys. *81*, 199-222, (1995).

Ramakrishnan, T. S. and Cappiello, A., A new technique to measure static and dynamic properties of a partially saturated porous medium, Chem. Eng. Sci., *46*, 1157-1163, (1991).

Schwartz, L. M., Martys, N., Bentz, D. P., Garboczi, E. J., and Torquato, S., Cross-property relations and permeability estimation in model porous media, Phys. Rev. E, *48*, 4584-4591, 1993.

Schwartz, L. M., Auzerais, F. M., Dunsmuir, J., Martys, N., Bentz, and Torquato, S., Transport and diffusion in three dimensional composite media, Physica A *207*, 28-36, 1994.

Spanne, P., Throvert, J. F., Jacquin, C. J. Lindquist, W. B., Jones, K. W., and Adler, P. M., Synchrotron computed microtomography of porous media: topology and transports, Phys. Rev. Letters, *73*, 2001-2004, 1994.

F. M Auzerais, T. S. Ramakrishnan, and L. M. Schwartz, Schlumberger-Doll Research, Ridgefield, CT 06877

J. Dunsmuir, Exxon Research and Engineering Company, Route 22 East, Annandale, NJ 08801

B. Ferréol, Elf Aquitaine, Departement Techniques et Specialites, Division Gisement, CSTJF, Avenue Larribeau, 64000 Pau France

N. Martys, National Institute of Standards and Technology, Building Materials Division, Gaithersburg, MD 20899

J. Olson and D. H. Rothman, Department of Earth, Atmospheric, and Planetary Sciences, Massachusetts Institute of Technology, Cambridge, MA 02139

(received June 30, 1995; accepted September 5, 1995.)